Astronomy & Astrophysics manuscript no.
(DOI: will be inserted by hand later)

March 16, 2005

Search for Spectral Evolution in high-redshift Supernovae

G. Garavini[1,2], G. Folatelli[2], S. Nobili[1,2], G. Aldering[4], R. Amanullah[2], P. Antilogus[1], P. Astier[1], G. Blanc[6], M. S. Burns[7], A. Conley[4], S. E. Deustua[9], M. Doi[10], R. Ellis[11], S. Fabbro[12], V. Fadeyev[4], R. Gibbons[4], G. Goldhaber[4,8], A. Goobar[2], D. E. Groom[4], I. Hook[13], D. A. Howell[5], N. Kashikawa[14], M. Kowalski 4, N. Kuznetsova 4, A. G. Kim[4], R. A. Knop[15], B. C. Lee[4], C. Lidman[3], J. Mendez[16,17], T. Morokuma[10], K. Motohara[10], P. E. Nugent[4], R. Pain[1], S. Perlmutter[4,9], V. Prasad[4], R. Quimby[4], J. Raux[1], N. Regnault[1], P. Ruiz-Lapuente[18], G. Sainton[1], B. E. Schaefer[18], K. Schahmaneche[1], E. Smith[15], A. L. Spadafora[4], V. Stanishev[2], R. C. Thomas4,, N. A. Walton[19], L. Wang[4], W. M. Wood-Vasey[4], and N. Yasuda[20]

(The Supernova Cosmology Project)

[1] LPNHE, CNRS-IN2P3, University of Paris VI & VII, Paris, France
[2] Department of Physics, Stockholm University, Albanova University Center, S-106 91 Stockholm, Sweden
[3] European Southern Observatory, Alonso de Cordova 3107, Vitacura, Casilla 19001, Santiago 19, Chile
[4] E. O. Lawrence Berkeley National Laboratory, 1 Cyclotron Rd., Berkeley, CA 94720, USA
[5] Department of Astronomy and Astrophysics, University of Toronto, 60 St. George St., Toronto, Ontario M5S 3H8, Canada
[6] Osservatorio Astronomico di Padova, INAF, vicolo dell'Osservatorio 5, 35122 Padova, Italy
[7] Colorado College, 14 East Cache La Poudre St., Colorado Springs, CO 80903
[8] Department of Physics, University of California Berkeley, Berkeley, 94720-7300 CA, USA
[9] American Astronomical Society, 2000 Florida Ave, NW, Suite 400, Washington, DC, 20009 USA.
[10] Institute of Astronomy, School of Science, University of Tokyo, Mitaka, Tokyo, 181-0015, Japan
[11] California Institute of Technology, E. California Blvd, Pasadena, CA 91125, USA
[12] CENTRA-Centro M. de Astrofísica and Department of Physics, IST, Lisbon, Portugal
[13] Department of Physics, University of Oxford, Nuclear & Astrophysics Laboratory, Keble Road, Oxford, OX1 3RH, UK
[14] National Astronomical Observatory, Mitaka, Tokyo 181-0058, Japan
[15] Department of Physics and Astronomy, Vanderbilt University, Nashville, TN 37240, USA
[16] Isaac Newton Group, Apartado de Correos 321, 38780 Santa Cruz de La Palma, Islas Canarias, Spain
[17] Department of Astronomy, University of Barcelona, Barcelona, Spain
[18] Louisiana State University, Department of Physics and Astronomy, Baton Rouge, LA, 70803, USA
[19] Institute of Astronomy, Madingley Road, Cambridge CB3 0HA, UK
[20] Institute for Cosmic Ray Research, University of Tokyo, Kashiwa, 277 8582 Japan

Abstract. A quantitative comparison of low and high-redshift Type Ia supernovae spectra observed at VLT is presented. Measurements of the Ca II H&K expansion velocity and equivalent widths of 12 high-redshift supernovae ($0.212 < z < 0.912$) are found to be statistically consistent with those of a sample of nearby supernovae. With this small sample, we find no evidence for evolution in the spectral properties of SNe Ia with redshift. One supernova, SN 2002fd, (z=0.279) is found to show spectral characteristics similar to peculiar SN 1991T/SN 1999aa-like SNe.

1. Introduction

Type Ia supernovae (SNe Ia) have been proven excellent distance indicators and their use has revealed the acceleration of the expansion of the universe (Perlmutter et al. 1998; Garnavich et al. 1998; Schmidt et al. 1998; Riess et al. 1998; Perlmutter et al. 1999; Knop et al. 2003; Tonry et al. 2003; Barris et al. 2004; Riess et al. 2004). Recently several new large projects have started, aiming at constraining the nature of dark energy through the measurement of the equation of state parameter. The control of the systematic uncertainties is critical to the success of these projects. Among them testing that Type Ia SNe do not evolve with redshift is essential.

The spectral energy distribution provides an avenue for testing this assumption. For example, the average metallicity of the Universe increases with cosmic time, so it is not unreasonable to expect that high-redshift SNe Ia are in environments that have lower metallicity. The effect on the spectral energy distribution of a lower metallicity progenitor has been modeled by Hoeflich et al. (1998) and Lentz et al. (2000). These studies find that such SNe Ia, especially at early epochs, are expected to show enhanced flux in the UV, weaker absorption features

Send offprint requests to: G. Garavini , garavini@in2p3.fr

in the optical and a shift in the minima of optical features to redder wavelengths.

With the large number of well-observed low-redshift supernovae now available, a wide range of spectral diversities is being found (see e.g Branch (2003)). The physical origin of these differences and their possible drift as a function of redshift are still not completely understood. Statistical studies are useful to probe for differences between high and low-redshift SN data sets. So far, very few distant SN Ia spectra have been compared with low-redshift data sets in a systematic manner (Perlmutter et al. 1998; Coil et al. 2000; Barris et al. 2004; Riess et al. 2003; Blakeslee et al. 2003; Matheson et al. 2004; Hook 2005).

Moreover, very few of the spectroscopically confirmed high-redshift SNe Ia have been reported as peculiar. The lack of SN 1991T/SN 1999aa-like SNe in the high redshift datasets could be due to the difficulty in identifying such SNe in what is generally low S/N spectra. Alternatively, it could be a sign of evolution (Li et al. 2001b,a). However, the number of published high redshift SNe Ia spectra is still small (several tens). The identification of SN 1991T/SN 1999aa-like supernovae at high-redshift is an important step in demonstrating that the range of SNe Ia that are observed at low-redshifts is also observed at high-redshifts.

During 2000, 2001 and 2002, the Supernova Cosmology Project (SCP) obtained the spectra of 20 high-redshift SNe Ia with FORS2 on the ESO Very Large Telescope (Lidman et al. 2005). In this paper, we analyze the 14 spectra with the highest signal-to-noise ratios and we perform a quantitative comparison between these spectra and the spectra of low-redshift SNe. We also develop an approach to identify SN Ia sub-types at $z \sim 0.5$. The paper is organized as follows. The dataset and identification scheme are presented in section 2. The comparison of high and low-redshift SNe are presented in section 3 together with a statistical analysis of the results.

2. Data set and Supernova Identification

2.1. The high-redshift spectroscopic data set

The supernova spectra that are analyzed in this work were obtained as part of a study by the SCP to discover and follow a large number of SNe Ia over a wide range of redshifts. Out of the 20 spectrally confirmed SNe Ia in Lidman et al. (2005), we select the 12 SNe Ia (z=0.212-0.912) with the highest signal-to-noise ratios (S/N per 20 Å resolution element greater than 3) to pursue the quantitative analysis that is presented below. One supernova, SN 2001go, was observed at three epochs, so there are 14 spectra in total.

The spectra, re-binned to 20 Å per pixel, are shown in Fig. 1, and the properties are summarized in Table 1. A full description of the observations and the data reduction are given in Lidman et al. (2005). Special care was taken in estimating the statistical error spectrum. It was estimated from regions free of SN and host galaxy light on the sky-subtracted two dimensional spectrum. The error spectrum is used to estimate the statistical uncertainties on the quantities we compute in the following analysis.

High-redshift supernova spectra usually suffer from host galaxy contamination. On the 2d spectra, the host galaxy and the SN Ia are usually spatially unresolved, making it difficult to estimate the contribution of the host to the observed flux. We estimated this contribution using a template matching technique based on a large set of nearby supernovae spectra and galaxy models similar to that used in Lidman et al. (2005). The estimated galaxy contamination, relative to the observed spectrum, are tabulated in column 10 of Table 1.

The epochs with respect to the B–band maximum light – reported in table 1 – were estimated using the preliminary light curve, if available, and/or spectroscopic dating by template matching with low-z SNe. The two methods usually agree within two days (Hook 2005), therefore we take this to be the uncertainty on the quoted epoch whenever a light curve estimate of the maximum was not available. The redshift of the supernova, when quoted with 3 significant figures, was estimated from host galaxy lines visible in the SN spectrum. When this was not possible, the redshift was estimated from supernova spectral features, and is then quoted with 2 significant figures.

2.2. SN identification

The identification of low-redshift SN Ia relies primarily on the detection of the absorption feature at approximately 6150 Å due to Si II λ6355. At redshifts above 0.5, this characteristic feature is redshifted beyond the wavelength range of most optical spectrographs and the classification of the supernova has to rely on spectral features that lie at bluer wavelengths. Because of the low signal to noise ratio usually available in high-redshift supernova spectra, this approach is not always conclusive. In Hook (2005), it is shown that four different wavelength regions can be used to distinguish between SN Ia and core-collapse supernovae in this redshift range. The same regions can also be used to identify spectral peculiarities among SNe Ia as those found in SN 1991T/SN 1999aa-like or SN 1986G/SN 1991bg-like supernova. In Table 2, the characteristics of these four wavelength regions for different types and sub-types of supernovae are schematically reported. Each spectral feature is qualitatively described as *strong*, *weak* or *absent* based on the absorption strength and *broad* or *narrow* based on the wavelength span. In the absence of a procedure that is based on quantitative measurements, this scheme helps in identifying the SN type and, in the case of SNe Ia, the sub-type.

2.3. SN 2002fd: A SN 1991T/SN 1999aa-like Supernova

SN 2002fd is the only supernova in our data set that clearly deviates from a "normal Ia" (see table 2). Within the scheme described above, the spectrum of SN 2002fd is to similar the spectra of SN 1991T/SN 1999aa-like supernovae. The spectrum of SN 2002fd (re-binned to 20 Å per pixel) is shown in Fig. 2 where it is compared to other well known peculiar and normal SN Ia. The 'Ca II H&K' feature in SN 2002fd is weaker than the same feature in normal SNe Ia, but stronger than the same feature in SN 1991T-like SNe Ia. The 'Fe II' and 'S II

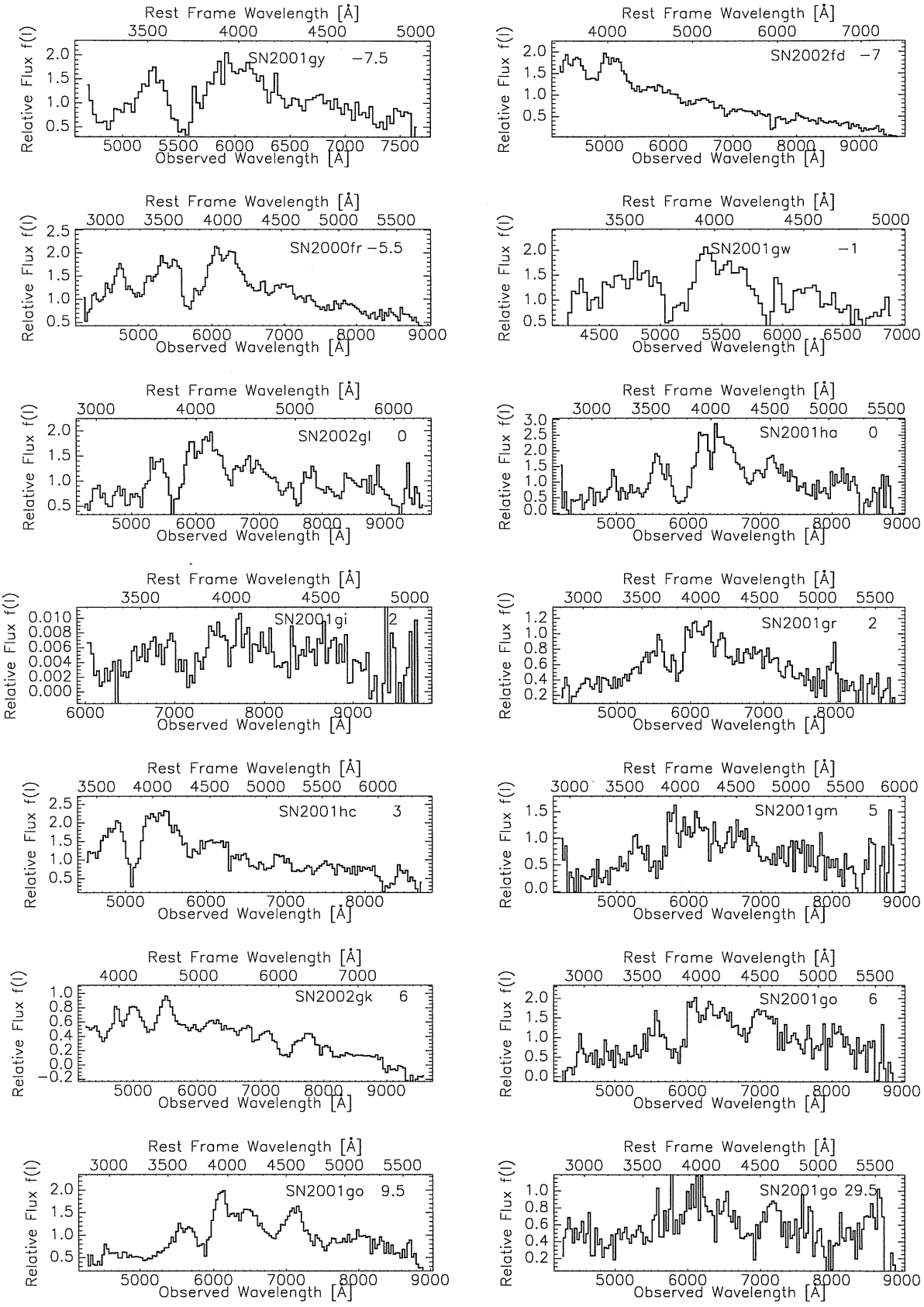

Fig. 1 The spectra of the high-redshift SNe Ia. Each spectrum is the original observed spectrum re-binned to 20 Å per pixel. See also Table 1

Table 1 A summary of the high-redshift data. For each SN, the redshift, the Modified Julian Date (MJD), the epoch since B-band maximum light, the telescope, the instrument, the instrument setting, the exposure time, the signal-to-noise ratio (per 20 Å bin), the percentage of galaxy contamination and SN Ia sub-type are given. See text for details.

SN-name	Red-shift[a]	Date (MJD)	Days from[b] B-band Maximum	Instrument	setup	telescope	Exposure time (s)	S/N[c]	Galaxy[d] %	ID
SN 2001gy	0.511	52021.3	-7,5(1)	FORS1	300V grism + GG435	VLT-UT1	2400	11	20	Ia
SN 2002fd	0.279	52376.1	-7(2)	FORS2	300V grism + GG435	VLT-UT4	600	46	28	Ia-pec
SN 2000fr	0.543	51676.2	-5.5(1)	FORS1	300V grism + GG435	VLT-UT1	7200	21	16	Ia
SN 2001gw	0.363	52021.4	-1(2)	FORS1	300V grism + GG435	VLT-UT1	1200	8	19	Ia
SN 2001ha	0.58	52022.0	0(2)	FORS1	300V grism + GG435	VLT-UT1	3600	4	6	Ia
SN 2002gl	0.510	52413.1	0(2)	FORS2	300V grism + GG435	VLT-UT4	3000	9	23	Ia
SN 2001hc	0.35	52022.1	0(2)	FORS1	300V grism + GG435	VLT-UT1	1800	14	14	Ia
SN 2001gr	0.540	52021.0	2(2)	FORS1	300V grism + GG435	VLT-UT1	3600	5	57	Ia
SN 2002gi	0.912	52407.2	2(2)	FORS1	300I grism + GG435	VLT-UT3	7200	3	37	Ia
SN 2001gm	0.478	52021.3	5(2)	FORS1	300V grism + GG435	VLT-UT1	2400	3	28	Ia
SN 2001go	0.552	52021.3	5.6(1)	FORS1	300V grism + GG435	VLT-UT1	2400	5	13	Ia
SN 2002gk	0.212	52413.3	6(2)	FORS2	300I grism + GG435	VLT-UT4	900	34	66	Ia
SN 2001go	0.552	52027.1	9.5(1)	FORS1	300V grism + GG435	VLT-UT1	7200	10	19	Ia
SN 2001go	0.552	52058.1	29.5(1)	FORS1	300V grism + GG435	VLT-UT1	9000	4	53	Ia

[a]The redshift is quoted to three significant figures if it is determined from host galaxy lines, otherwise two.

[b]Uncertainties are quoted in parenthesis

[c]For a 20 Å bin element

[d]Estimated contribution of the host to the total flux.

Table 2 A description of the spectroscopic features used to type SN at $z \geq 0.5$. Four wavelength regions are selected for performing the SN typing. Each spectral feature, in these regions, is qualitatively described as *strong*, *evident*, *weak* or *absent* based on the absorption strength and *broad* or *narrow* based on the wavelength span.

Region Id	λ-Region Rest Frame[Å]	Normal Type Ia	91T/99aa-like	91bg/86G-like	Type Ib/c	Type II
'Ca II H&K'[g]	3550-3950	strong/broad	weak or absent/broad[a,b]	strong/broad	evident/broad[c]	absent
'Si II'[d]	3950-4100	evident/narrow[b]	weak[a,b]	absent	absent	absent
'Fe II'[e,f]	4600-5200	strong/broad	strong/narrow[a]	strong/broad	strong/broad	absent[h]
'S II W'	5200-5600	strong/narrow[a,b]	weak or absent[a]	strong/narrow[a,b]	absent	absent

[a]Before maximum light

[b]Around maximum light

[c]A few peculiar exceptions.

[d]Marks the beginning of the distinctive strong Ti II absorption feature in 91bg/86G-like SNe Ia.

[e]In Normal Ia characteristic line profile time evolution.

[f]Dominated by Fe III in pre-maximum spectra of 91T/99aa-like SNe Ia.

[g]Splitted minimum in some Ia.

[h]In Type II SNe, the H_β line lies on the blue side of the "FeII" region.

W' regions are similar to those in SN 1999ac (Garavini 2005). Given the low-redshift, Si II λ 6355 is also visible. This feature in SN 2002fd is intermediate in strength to the strength of this feature SN 1999aa and SN 1999ac/normal SNe. From this qualitative analysis of the spectrum, we classify SN 2002fd as a peculiar SN 1991T/SN 1999aa-like object with characteristics in between the extreme SN 1991T-like SNe and normal SNe (e.g. SN 1994D). It is similar to SN 1999aa. In section 3.4, we show that the equivalent widths of the absorption features in SN 2002fd are also consistent with those found at low redshift for the SN 1991T/SN 1999aa-like objects.

Finding SNe with spectral characteristics similar to those of SN 1999aa at the redshift of SN 2002fd gives us confidence that supernova populations at low and intermediate z are the same. SN 1991T/SN 1999aa-like supernovae appear to make up 20% of all supernovae observed at low-z (Li et al. 2001b) although this high peculiarity rate could be the result of the difficulty to classify spectroscopically peculiar SN 1999aa-like

reword more gentle

Do you mean at high-redshift? Why would this difficulty make the rate high?

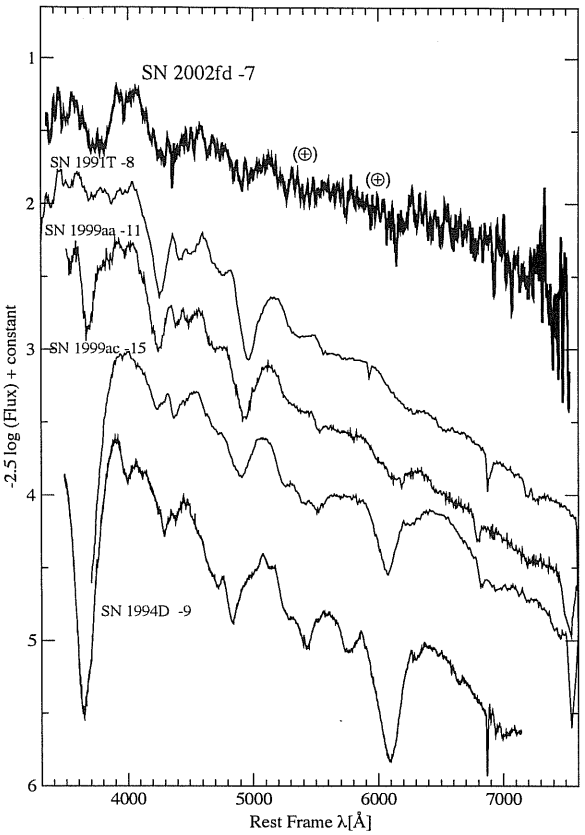

Fig. 2 SN 2002fd at day -7, re-binned to 20 Å per pixel (thick solid line), compared to normal and peculiar SNe. The ⊕ symbols mark regions of strong telluric absorption.

SNe (Branch 2001). Nevertheless, we should find some of these SNe at high-redshift. Li et al. (2001b) used a Monte-Carlo simulation to estimate that, in a magnitude-limited high-redshift supernova search, where SN 1991T/SN 1999aa-like SNe suffer an additional extinction of 0.4 magnitudes, between 18.6% and 6% (for an age bias of +7 and −1 days respectively) of all high-redshift SNe should be SN 1991T/SN 1999aa-like SNe.

The precise number depends on the details of the methods that are used in the search. Many SN 1991T/SN 1999aa-like SNe may have already been observed at high-redshift but not clearly identified because the signal-to-noise ratio in the spectrum was too low or the light-curve was not exceptionally broad. It is becoming clearer that SN 1991T/SN 1999aa-like SNe do not always have broad light curves and vice-versa, see for example SN 1999ee (Hamuy et al. 2002), SN 2002cx(Li et al. 2003) or SN 1999aw (Strolger et al. 2002). SN 2002fd is one of the first examples of a SN 1991T/SN 1999aa-like supernova in the Hubble flow, and its discovery demonstrates that these objects are also found at higher redshifts. Of course, larger data samples are required to check whether the fraction of peculiar high-redshift SNe is consistent with that found in the low-redshift Universe or if there is an evolution in the relative fractions with redshift that could affect the results derived in cosmology.

3. Comparing High and Low-redshift spectra

In this section, we compare our high-redshift spectra with spectra from a broad sample of low-redshift supernovae in order to probe for possible differences between the low and high-redshift populations. We first perform a qualitative analysis (sections 3.1 and 3.2) and then turn to a more quantitative approach (section 3.3). The measured values are reported in Table 4.

3.1. Velocities

For normal SNe Ia, the velocity of Ca II H&K drops rapidly, from values around 22000 km/s before maximum light to 14000 km/s at maximum light. After maximum light, the rate of decrease slows and the velocity decreases by about 4000 km/s in 50 days. The mean trend for normal SNe Ia, from 10 days before maximum light to 40 days after maximum light, is shown in Fig. 3. The shaded area represents the dispersion (one standard deviation about the mean). The trend and the dispersion have been computed from a large sample of nearby supernova (Garavini et al. 2004).

The inferred expansion velocity of the ejecta in underluminous SNe is lower than the expansion velocity in normal SNe (Leibundgut et al. (1993); Wells et al. (1994); Patat et al. (1996); Garnavich et al. (2001); Li et al. (2003)). The differences are more pronounced in the case of the Si II λ6355 absorption feature where differences of more than 2000 km s^{-1} are seen (Branch & van den Bergh 1993). The separation is less conspicuous for the Ca II H&K absorption – measurable in the redshift range of our data set – but the trend remains, as can be seen in Fig. 3 where SN 1999by (Garnavich et al. 2001) and SN 1991bg (Leibundgut et al. 1993)) are plotted with the dashed and dotted lines, respectively. Assuming that intrinsically low-luminosity high-redshift SNe show the same spectral characteristics of those in the local universe, measured expansion velocities values on the lower edge of the distribution shown in Fig. 3, would suggest a possible under-luminous SN.

The velocities of both the low-redshift and high-redshift SNe are measured by performing an error-weighted non-linear least-squares fit to the whole line profile. The line profile is modeled with a Gaussian and the continuum over the width of the line is modeled as a straight line. All the SNe in our data set were measured, with the exception of SN 2001gk, for which the line profile is incomplete, and SN2001go at +29 days, for which the signal to noise is too low to correctly identify the absorption. The uncertainty in the redshifts is taken to be 300 km/s if the redshift was estimated from galaxy lines. For SN 2001ha and SN 2001hc, we could not identify host galaxy lines, so their redshifts were estimated by comparing their spectra with the spectra of nearby SNe Ia. In these cases the uncertainty is increased to 3000 km/s. These uncertainties dominate the uncertainties from the fit.

The velocity of the Ca II H&K feature in all our high-redshift supernovae lie above the dashed line in Fig. 3, which represents the velocity of this feature in the peculiar underluminous SN 1999by. We note that the velocities of our high-

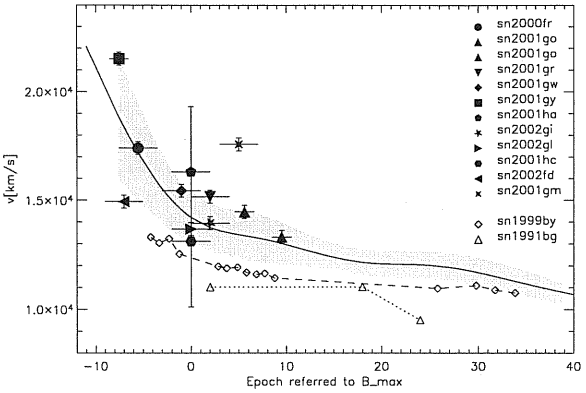

Fig. 3 The change in the velocity of the Ca II H&K feature with epoch for a sample of high-redshift SNe (presented in section 2, filled symbols) and a sample of low-redshift SNe. The dashed and dotted lines indicate the values of extremely under-luminous SNe SN 1999by (Garnavich et al. 2001) and SN 1991bg (Leibundgut et al. 1993) respectively. The solid line indicates the average trend for Ca II H&K, which has been computed using a large data set of low-redshift normal SNe Ia. The gray band shows the dispersion (1 standard deviation) of the data about the average trend.

redshift SNe are consistent with those of spectroscopically normal SNe. A similar result was obtained by Hook (2005). Li et al. (2001b), estimated that 16% of all supernovae discovered in the local universe are under-luminous. However, for magnitude-limited high-redshift supernova searches – as those carried out by the SCP – there is a bias against discovering SN 1991bg-like SNe. Thus, the lack of any such SNe in our high-redshift SNe sample is not unexpected.

3.2. Equivalent Widths

Folatelli (2004b) defined quantities that are similar to the equivalent widths that are used in stellar spectroscopy. However, as they pointed out, in the case of supernova spectra the relationship between these quantities and the physical conditions of the ejecta is complex. However, this does not prevent us from using these well defined quantities when comparing nearby and distant SN Ia spectra. In the rest of this paper, we will refer to these quantities as equivalent widths EWs.

In the original definition given by the authors an absorption feature is a wavelength region bounded by local spectral flux maxima. Figure 4 shows these regions as they are defined at different epochs. Each feature is marked with a number from 1 to 8 and each number corresponds to a label mnemonic name. The spectra of the high-redshift SN Ia generally cover only regions 1 to 5. The ranges over which the upper and lower limits of features are defined are given in Table 3. These limits vary in time, and from SN to SN.

The continuum is computed as the straight line fit through the two local maxima that bound a feature[1] (see panel (**b**) in Fig. 4). The definition of the continuum and the identification of the local maxima in high redshift SN spectra can be challenging because of the generally noisy data. The measurement technique adopted in this work is described in sec. 3.2.1.

Once the continuum is traced, the EW is computed for each feature within its wavelength limits. The spectrum is divided by the continuum and the resulting area of the feature is measured (in units of Å). In this case, the calculation was approximated by a simple rectangular integration method:

$$\mathrm{EW} = \sum_{i=1}^{N} \left(1 - \frac{f_\lambda(\lambda_i)}{f_c(\lambda_i)}\right) \Delta\lambda_i, \qquad (1)$$

where λ_i ($i = 1, \ldots, N$) are the central wavelength values of bins of size $\Delta\lambda_i$ over the span of the feature; $f_\lambda(\lambda_i)$ is the measured flux in each bin i; $f_c(\lambda_i)$ is the fitted continuum flux evaluated at the same points. Deviating points due to bad pixels or narrow host-galaxy lines were rejected using a 3σ-clipping algorithm.

Table 3 Feature limits.

Feature ID	Mnemonic Label	Blue-ward limit range (Å)	Red-ward limit range (Å)
1	"Ca II H&K"	3500 – 3800	3900 – 4100
2	"Si II 4000"	3900 – 4000	4000 – 4150
3	"Mg II 4300"	3900 – 4150	4450 – 4700
4	"Fe II 4800"	4500 – 4700	5050 – 5550
5	"S II W"	5150 – 5300	5500 – 5700
6	"Si II 5800"	5550 – 5700	5800 – 6000
7	"Si II 6150"	5800 – 6000	6200 – 6600
8	"Ca II IR"	7500 – 8000	8200 – 8900

3.2.1. Measurement technique

The technique used to measure equivalent width in SN Ia was extensively described in the original works Folatelli (2004b) and Folatelli (2004a) together with a detailed study of the possible systematic effects. For completeness in this section we schematically summarize the topical points to the application of this technique to high red shift supernova spectra.

To measure the EW of a spectral feature the local continuum must be determined. To perform this operation we proceeded as following:

- The two local maxima that bound the absorption feature are visually identified.
- A small wavelength region (to which hereafter we refer to as fitting region) is selected around each identified maximum[2], always within the wavelength ranges of Table 3.
- To the data extracted from both fitting regions, we fit a straight line.
- The result of the fit is taken as the continuum and used as an input in Eq. 1.

[1] The chosen maxima are the ones that maximize the wavelength span of the feature with the restriction that the derived continuum does not intersect the spectrum within the feature limits and the possible exception of noise artifacts in case of low signal to noise ratio data.

[2] See panel (**b**) in Fig. 4, the four vertical lines represent an example of the wavelength span of each fitting region.

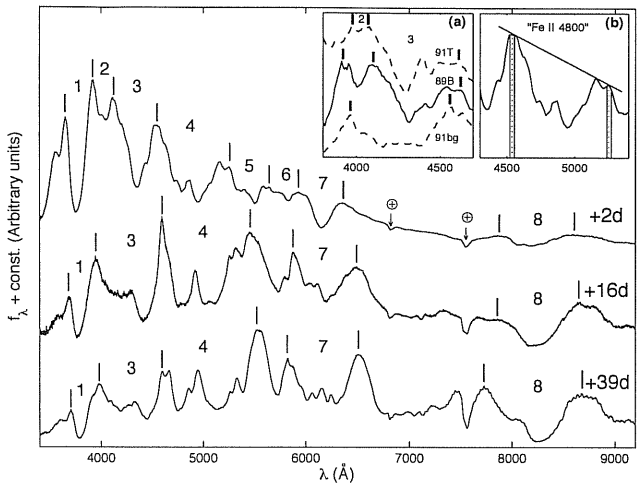

Fig. 4 SNe Ia spectral evolution and feature definitions for three epochs: 2, 16 and 39 days after maximum light. Numerical labels correspond to the following adopted feature names: **1**- "Ca II H&K"; **2**- "Si II 4000"; **3**- "Mg II 4300"; **4**- "Fe II 4800"; **5**- "S II W"; **6**- "Si II 5800"; **7**- "Si II 6150"; and **8**- "Ca II IR". Short vertical lines show the approximate positions where the continuum is taken in each case. Feature ranges change with time and, due to blending, some weaker features are not considered at later epochs. Note that, as the SNe leave the photospheric phase, continuum points correspond to emission peaks. *Panel* (**a**): the region of features #2 and #3 for near-maximum spectra of SN 1991T (top), SN 1989B (middle), and SN 1991bg (bottom). Feature #2 is not defined in the case of 1991bg-like SNe. Adopted feature limits are marked with vertical lines. *Panel* (**b**): an example of the continuum trace for "Fe II 4800" on a Branch normal SN near the time of maximum light. Here, solid vertical lines show the regions where the continuum is fitted. Dotted lines mark the measurement limits.

This approach was chosen as a practical one to be consistently used both for high and low signal to noise ratio data. This requirement is crucial for carrying out the comparison between EW's of low and high redshift supernova spectra presented in sec. 3.2.3.

The correct identification of the local maximum can be the source of systematic uncertainties. This were taken into account as reported in the following section. The wavelength span of the two fitting regions depends on the signal to noise ratio (SNR) of the spectrum. In high SNR spectra the maxima are easily identifiable and small regions (typically less than 10 Å wide) give the best estimate of the peak. In relatively low SNR spectra, as those presented in this work, larger regions (typically 20 Å wide) are needed to estimate at best the local maximum flux. Large wavelength span would tend to set a lower continuum level and thus to produce EW systematically biased toward smaller values.

3.2.2. Possible systematic effects

Because of the required visual identification of the maxima in low SNR data, different observers would tend to select fitting regions differing both in wavelength span and location. Possible systematic uncertainties arising from the selection of the region around each maximum were accounted for by Monte-Carlo simulations. Each identified fitting region was randomly varied in wavelength span according to a Gaussian distribution with $\sigma = l/4$, where l is the original span of the fitting region (typically $l = 20$ Å). In addition the position, in lambda space, of the region was randomly shifted according to a Gaussian distribution with $\sigma = 10$Å. The two effects were taken into account simultaneously. The σ of the simulations were chosen in a conservative manner so to take into account even large miss-identification. The standard deviation of the measurements so obtained was taken as systematic uncertainty associated with the measured value (see sec. 3.2.3).

The systematic effect of low signal to noise ratio was also tested by adding Gaussian noise to high-quality spectra with known EW. No significant bias was detected on the resulting EW values.

Further systematic effects could arise from the removal of the host-galaxy light contamination. Residual galaxy light underlying the SN spectrum would bias the EW measurements toward low values. A too large amount of galaxy light removed from the SN spectrum would, instead, bias the EW measurements toward high values. This effect must be taken into account. A Montecarlo simulation was performed to establish the accuracy of the host galaxy removal technique used. This was estimated to be of about 10% of the input galaxy light. The corresponding systematic uncertainty in the EWs was computed as in Folatelli (2004b).

3.2.3. EW measurements

Because of the moderate signal to noise ratio of our spectra, we focused our analysis on the three strong absorption features labeled (see Table 3) "Mg II 4300", "Fe II 4800" and "Ca II H&K".

In Figures 5, 6 and 7, we compare the strengths of these features in high and low-redshift SNe. Both samples were measured according to the recipe presented in Folatelli (2004b) and summarized in sec. 3.2.1. Since the EWs of these features are a strong function of the phase, the EWs are plotted with respect to B-band maximum light. In Figs. 5 and 6 the solid line indicates the mean trend of the EW for normal SNe Ia, while the gray, filled region represents the dispersion (one standard deviation about the mean trend) as described in Folatelli (2004b)). Note, that the plotted errors bars in the EW's of the high-redshift SNe Ia include both statistical uncertainties, from the measurement, and systematic uncertainties from residual host galaxy contamination but do not include that from possible misidentification of the maxima around the absorption feature (i.e. misidentification of the fitting regions). Table 4 reports the measured EW values, their uncertainties are reported between parentheses; The first value in the parentheses includes only statistical and host galaxy contamination uncertainties, the second includes also the possible fitting regions uncertainties added in quadrature.

At around one week after maximum light, the EW of "Mg II 4300" (Fig 5) suddenly increases from ~100Å to ~250Å on time scales of less than a week. Over this time-scale, the

Table 4 Measurements of the velocities of Ca II H&K and of the EWs of Ca IIH&K, Mg II and Fe II. Measurements errors are reported in parenthesis, the first value includes statistical plus host galaxy contamination uncertainties, the second value includes (added in quadrature) also the possible systematic uncertainties due to misidentification of the fitting regions, (see sec. 3.2.2 for details).

SN	day	Ca HK vel	Ca II H&K EW	Mg II EW	Fe II EW
sn2001gy	-7.5 (1)	21520 (300)	176 (8/21)	111 (12/31)	
sn2002fd	-7 (2)	14940 (300)	73.6 (3/14)	101 (8/11)	86 (15/23)
sn2000fr	-5.5 (1)	17400 (300)	122 (13/14)	103 (6/13)	91 (13/23)
sn2001gw	-1 (2)	15440 (300)	130 (9/13)	125 (17/22)	
sn2002gl	0 (2)	13680 (300)	124 (14/15)	121 (12/18)	168 (20/25)
sn2001ha	0 (2)	16310 (300)	188 (19/22)	132 (9/24)	216 (33/62)
sn2001hc	0 (2)	13110 (300)	112 (15/15)	116 (11/18)	140 (15/23)
sn2002gi	2 (2)	13950 (300)			
sn2001gr	2 (2)	15170 (300)	94.6 (10/22)	140 (16/34)	141 (31/69)
sn2001gm	5 (2)	17580 (300)	128 (23/26)	123 (17/40)	169 (34/84)
sn2001go	5.6 (1)	14470 (300)	120 (11/28)	93 (11/24)	191 (28/41)
sn2002gk	6 (2)		91 (6/11)	161 (14/16)	157 (16/17)
sn2001go	9.5 (1)	13320 (300)	112 (6/13)	181 (14/24)	174 (20/27)
sn2001go	29.5 (1)			228 (22/48)	315 (41/52)

Mg II 4300" feature deepens and blends with the neighboring "Si II 4000" feature. The actual phase at which this sudden increase takes place depends on the intrinsic luminosity of the SNe: for under-luminous SNe Ia it seems to occur as early as 5 days before maximum light, while, for normal SNe Ia it occurs around one week after maximum light, and, for SN 1991T/SN 1999aa-like objects, it occurs later than day +10. (Folatelli 2004b). Thus, the "Mg II 4300" feature can be used to discriminate between different Type Ia sub-types. The EWs of the high-redshift supernovae (all except SN 2002gi are measured) are consistent with the trend defined by low-redshift supernova values within 2-σ. Moreover, SN 2001go, for which measurements at three epochs are available, shows the sudden increase at around one week after maximum, as do most low-redshift normal SNe.

We note that the EW of the 'Mg II 4300' feature for high-redshift SNe Ia, before maximum light, are on average higher than the mean trend of low redshift SNe. This could be due to the possible systematic uncertainties in the identification of the fitting region in early spectra when this feature is less deep. However, all points are within 2-σ from the model describing local SNe and a simple χ^2 test shows that the deviation is not statistically significant as will be clear in section 3.3.

The trend in the EW of "Fe II 4800" is the same for all SN Ia sub-types (see Fig. 6). EWs increase from around 100Å before maximum light to 350Å two weeks after. All SNe (with the exception of SN 2001gu, SN 2001gw, SN 2001gy and SN 2002gi, for which the absorption feature was not easily identifiable), were measured and were found to be well within the intrinsic spread of low-redshift supernovae.

The trend in the EW of "Ca II H&K" is shown in Fig. 7. The distribution of points is less homogeneous than that of other features, especially before maximum light, so the mean trend was not modeled in Folatelli (2004b). Instead, the portion of the plot where most low-redshift normal and under-luminous SNe are located is indicated, for clarity, by a gray-filled region. However, some outliers are found among normal SNe and these are indicated with the small diamond symbols. The overall intrinsic spread in this EW is the largest of all the features analyzed in this work. Before maximum light, peculiar SN 1991T-like objects show systematically low values, as indicated by the small square symbols. The high-redshift supernovae (all except SN 2002gi are plotted) do not show significant deviations with respect to the low-redshift sample shown in the plot.

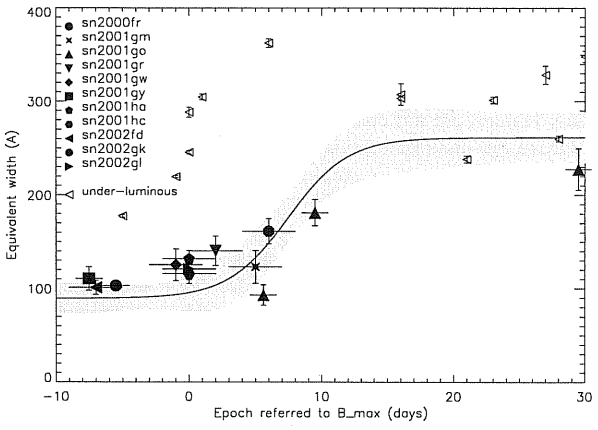

Fig. 5 A comparison between the 'Mg II 4300' EWs in low- and high-redshift SNe Ia. High-redshift supernova are indicated by large filled symbols. The solid line indicates the mean trend for normal low-redshift SNe Ia, while the gray, filled region represents the dispersion (one standard deviation about the mean trend) as described in Folatelli (2004b)). Peculiar under-luminous SNe are shown separately for comparison.

3.3. Statistical comparison

In this section, a quantitative – statistical – comparison of the low- and high-redshift SNe is performed using the spectral indicators described in section 3.2. Folatelli (2004b) modeled the mean trends in the EWs of the 'Fe II 4800' and 'Mg II 4300' features in normal – low-redshift – supernovae with cubic splines.

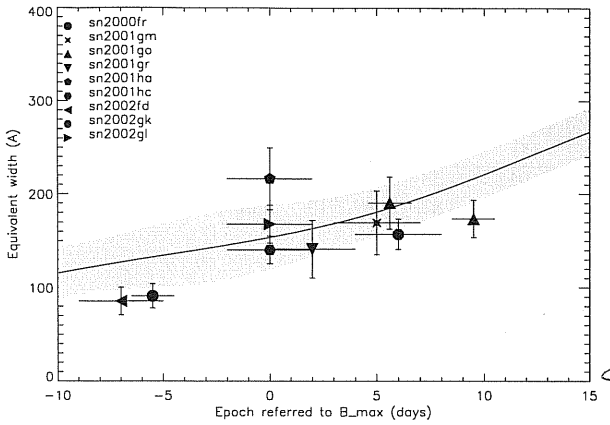

Fig. 6 A comparison between the 'Fe II 4800' EWs in low- and high-redshift SNe Ia. As in figure 5, high-redshift supernova are indicated by large filled symbols, the solid line marks the mean trend for normal low-redshift SNe Ia, while the gray, filled region represents the dispersion (one standard deviation about the mean trend) as described in Folatelli (2004b)

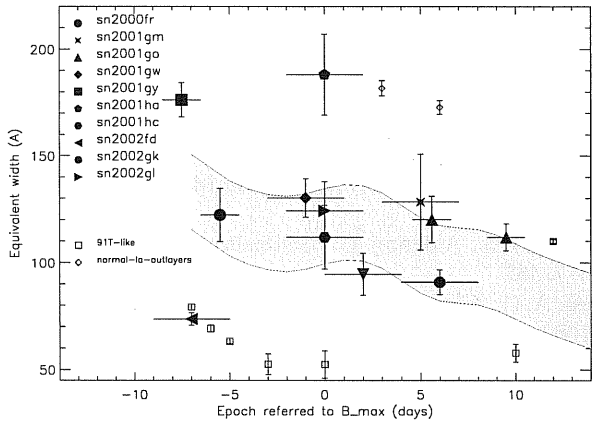

Fig. 7 A comparison between the 'Ca II H&K' EWs in low- and high-redshift SNe Ia. High-redshift supernova are indicated by large filled symbols. The location of most normal and under-luminous SNe is indicated by the gray filled region. However, some normal SNe, are outliers and these are indicated with the diamond symbols. Slow decliner SNe are indicated by the square symbols.

These models are plotted in Figs. 5 and 6 and they can be used to test if high-redshift supernovae EWs follow the same trends as low-redshift SNe.

The results of a χ^2 test is shown in Table 5. The intrinsic dispersion around the models for normal low-z supernovae – as quoted in Folatelli (2004b) – was added in quadrature to the statistic and systematic uncertainties to perform the test. The uncertainty on the x axis was propagated according to the EW model for normal low redshift SNe and added in quadrature to the measurements error on the EWs. The χ^2 test was repeated twice. Columns 1 to 4 in Table 5 report the result of the test when only the systematic uncertainty due to host galaxy subtraction was considered. Columns 4 to 8 report the result of the test when also the possible systematic uncertainties due to misidentification of the maxima (i.e. fitting regions misidentification) was included. It has to be noted that the fitting region uncertainties – included in this second test – should be considered as an upper limit to the possible systematic uncertainty due to the EW's measurement technique (see section 3.2.2 for details).

Columns 1, 2, 5 and 6 of Table 5 report the χ^2 referring to the comparison with the 'Fe II 4800' and 'Mg II 4300' EW models for normal supernovae, while columns 3, 4, 7 and 8 refer to the comparison with under-luminous SNe (e.g. SN 1986G and SN 1991bg).

The hypothesis that the EW measured on our high-redshift supernovae follow the same evolution as those measured on low redshift normal supernovae is statistically accepted. Thus, no sign of evolution with redshift is visible in our data set. Moreover, the hypothesis that EWs measured on our high-redshift supernovae are consistent with those of under-luminous low redshift SNe is rejected.

Lentz et al. (2000) claim that the strength of supernova absorption features should be affected by the drift toward lower metallicity progenitor expected at high-redshift. However, measuring the intrinsic spread of EWs of the absorption features of their models relative to those of the one solar metallicity synthetic spectrum, we found values lower than what is measured for the low-redshift supernovae. Thus, the range in which EW vary – studied in Folatelli (2004b) – is dominated by other effects than their prediction from metallicity variations. The possible change of rest frame U-B color in high-redshift SNe is probably a more sensitive parameter to investigate the effects of varying metallicity (Lentz et al. 2000).

3.4. The "Ca II H&K" EW of SN 2002fd

Prior to maximum light, the EW of Ca II H&K can be used to separate peculiar SN 1991T/SN 1999aa-like SN Ia from normal SNe Ia, see Fig. 7). If the identification of SN 2002fd as a peculiar object is correct, we expect the EW to be lower than that of normal SNe. The average EW prior to light curve maximum in normal SNe is $\langle EW \rangle = 114.1$ and the scatter around the mean value is $\sigma_{\langle EW \rangle} = 14.2$ For peculiar SN 1991T/SN 1999aa-like SNe we find $\langle EW \rangle = 68.7$ and $\sigma_{\langle EW \rangle} = 6.1$ The value measured for SN 2002fd, (EW = 73.6 ± 2.9), is consistent – within one standard deviation – with that found for SN 1991T/SN 1999aa-like SN Ia, and inconsistent (at ~2σ) with the normal SN.

4. Summary and Conclusions

Spectroscopic data of 12 high-redshift supernovae, in the redshift interval z=0.212 to 0.912, were analyzed and a qualitative classification scheme is proposed to classify high-redshift SN Ia. Based on this classification scheme, all our SNe, except SN 2002fd at z=0.27, were classified as normal SNe Ia. We also find that, based on spectral properties alone, none of the supernovae studied here were under-luminous.

A quantitative comparison between low and high-redshift SN Ia by means of spectral indicators has been presented. The velocities of the ejecta in high-redshift supernovae, as inferred

Table 5 The result of the χ^2 test comparing the EWs of high-redshift SNe with the models representing normal low-redshift SNe for 'Fe II 4800' and 'Mg II 4300' (column 1, 2, 4 and 5) and with values of under-luminous SNe (column 3, 4, 6 and 7). Columns 1 to 4 report the results including only the statistical and systematic uncertainties due to host galaxy subtraction. Columns 5 to 8 report the results when also the possible misidentification of fitting regions in included (see 3.2.2 and 3.3 for details).

Feature	χ^2/dof (1)	P_{norm} (2)	χ^2/dof (3)	P_{faint} (4)	χ^2/dof (5)	P_{norm} (6)	χ^2/dof (7)	P_{faint} (8)
Fe II	13.9/11	0.24	31.8/11	0.0008	7.2/11	0.78	18.33/11	0.07
Mg II	13.8/13	0.38	307.4/13	0.00	8.4/13	0.82	199.7/13	0.00

from the minimum of Ca II H&K feature, were compared to those of low-redshift SNe with the aim of uncovering differences. No differences could be found. The equivalent widths of "Fe II 4800", "Mg II 4300" and "Ca II H&K" in high-redshift SNe Ia are found to follow the same trends with epoch as those observed in low-redshift SNe. Furthermore, the equivalent widths of "Fe II 4800" and "Mg II 4300" in high-redshift SNe are found to be statistically consistent with the equivalent widths observed in low-redshift normal SNe.

Expansion velocity and equivalent widths are shown to be valuable means for comparing low and high-redshift supernova spectra thanks to the low minimal signal to noise ratio required to perform the measurements. The EWs of Ca II H&K in the spectrum of SN 2002fd are consistent with those observed in SN 1991T/SN1999aa-like objects in the local universe quantitatively confirming the sub-type identification of this SN and pointing out that this feature can be successfully used to identify peculiar object at high-redshift.

In the near future, when large data set of high redshift supernovae spectra will become available (e.g those derived from the SNLS[3] and ESSENCE[4] projects) statistical comparisons as those presented in this work will be able to further investigate supernova evolution with redshift.

References

Barris, B. J., Tonry, J. L., Blondin, S., et al. 2004, ApJ, 602, 571

Blakeslee, J. P., Tsvetanov, Z. I., Riess, A. G., et al. 2003, ApJ, 589, 693

Branch, D. 2001, PASP, 113, 169

Branch, D. 2003, astro-ph/0310685

Branch, D. & van den Bergh, S. 1993, AJ, 105, 2231

Coil, A. L., Matheson, T., Filippenko, A. V., et al. 2000, ApJ, 544, L111

Folatelli, G. 2004a, PhD Thesis U. Stockholm

Folatelli, G. 2004b, New Astronomy Review, 48, 623

Garavini, G., Folatelli, G., Goobar, A., et al. 2004, AJ, 128, 387

Garavini, G. e. 2005, submitted to AJ

Garnavich, P. M., Kirshner, R. P., Challis, P., et al. 1998, ApJ, 493, L53+

Garnavich, P. M. et al. 2001, astro-ph/0105490

Hamuy, M., Maza, J., Pinto, P. A., et al. 2002, AJ, 124, 417

Hoeflich, P., Wheeler, J. C., & Thielemann, F. K. 1998, ApJ, 495, 617

Hook, I. M. 2005, submitted to AJ

Knop, R. A., Aldering, G., Amanullah, R., et al. 2003, ApJ, 598, 102

Leibundgut, B., Kirshner, R. P., Phillips, M. M., et al. 1993, AJ, 105, 301

Lentz, E. J., Baron, E., Branch, D., Hauschildt, P. H., & Nugent, P. E. 2000, ApJ, 530, 966

Li, W., Filippenko, A. V., Chornock, R., et al. 2003, PASP, 115, 453

Li, W., Filippenko, A. V., & Riess, A. G. 2001a, ApJ, 546, 719

Li, W., Filippenko, A. V., Treffers, R. R., et al. 2001b, ApJ, 546, 734

Lidman, C., Howell, D. A., Folatelli, G., et al. 2005, A&A, 430, 843

Matheson, T., Blondin, S., Foley, R. J., et al. 2004, ArXiv Astrophysics e-prints

Patat, F., Benetti, S., Cappellaro, E., et al. 1996, MNRAS, 278, 111

Perlmutter, S., Aldering, G., della Valle, M., et al. 1998, Nature, 391, 51

Perlmutter, S., Aldering, G., Goldhaber, G., et al. 1999, ApJ, 517, 565

Riess, A. G., Filippenko, A. V., Challis, P., et al. 1998, AJ, 116, 1009

Riess, A. G., Strolger, L., Tonry, J., et al. 2004, ApJ, 607, 665

Riess, A. G., Strolger, L., Tonry, J., et al. 2003, astro-ph/0308185

Schmidt, B. P., Suntzeff, N. B., Phillips, M. M., et al. 1998, ApJ, 507, 46

Strolger, L.-G., Smith, R. C., Suntzeff, N. B., et al. 2002, AJ, 124, 2905

Tonry, J. L., Schmidt, B. P., Barris, B., et al. 2003, ApJ, 594, 1

Wells, L. A., Phillips, M. M., Suntzeff, B., et al. 1994, AJ, 108, 2233

[3] http://cfht.hawaii.edu/SNLS

[4] www.ctio.noao.edu/~ wsne